

CHEM MED CHEM

CHEMISTRY ENABLING DRUG DISCOVERY

Accepted Article

Title: A multi-step virtual screening protocol for identification of novel non-acidic microsomal prostaglandin E2 synthase-1 (mPGES-1) inhibitors

Authors: Suhaib Shekfeh, Burcu Çalışkan, Katrin Fischer, Tansu Yalçın, Ulrike Garscha, Oliver Werz, and Erden Banoglu

This manuscript has been accepted after peer review and appears as an Accepted Article online prior to editing, proofing, and formal publication of the final Version of Record (VoR). This work is currently citable by using the Digital Object Identifier (DOI) given below. The VoR will be published online in Early View as soon as possible and may be different to this Accepted Article as a result of editing. Readers should obtain the VoR from the journal website shown below when it is published to ensure accuracy of information. The authors are responsible for the content of this Accepted Article.

To be cited as: *ChemMedChem* 10.1002/cmdc.201800701

Link to VoR: <http://dx.doi.org/10.1002/cmdc.201800701>

WILEY-VCH

www.chemmedchem.org

A Journal of



FULL PAPER

A multi-step virtual screening protocol for identification of novel non-acidic microsomal prostaglandin E₂ synthase-1 (mPGES-1) inhibitors

Suhaib Shekfeh,^[a] Burcu Çalışkan,^[a] Katrin Fischer,^[b] Tansu Yalçın,^[a] Ulrike Garscha,^[b] Oliver Werz,^[b] and Erden Banoglu,^{*[a]}

[a] Dr. Suhaib Shekfeh; Assoc. Prof. Burcu Çalışkan; Tansu Yalçın; Prof. Erden Banoglu
Department of Pharmaceutical Chemistry
Faculty of Pharmacy, Gazi University
Ankara 06560, Turkey
E-mail: banoglu@gazi.edu.tr

[b] Katrin Fischer; Dr. Ulrike Garscha; Prof. Oliver Werz
Department of Pharmaceutical/Medicinal Chemistry
Institute of Pharmacy, Friedrich-Schiller-University Jena
Philosophenweg 14, D-07743 Jena, Germany

Supporting information for this article is given via a link at the end of the document.

Abstract: Microsomal prostaglandin E₂ synthase-1 (mPGES-1) is considered as potential therapeutic target for treatment of inflammatory diseases and certain types of cancer. In order to capture novel scaffolds for mPGES-1 inhibition, we applied a virtual screening protocol comprising molecular docking, fingerprints-based clustering with diversity-based selection, protein-ligand interactions fingerprints, and molecular dynamics (MD) simulations with Molecular Mechanics–Poisson Boltzmann Surface Area (MM-PBSA) calculation. The hits identified were carefully analyzed to ensure the selection of novel scaffolds, which make stable interactions with key residues in the mPGES-1 binding pocket and inhibit the catalytic activity of the enzyme. As a result, we discovered two promising chemotypes **6** and **8** as non-acidic mPGES-1 inhibitors with IC₅₀ of 1.2 and 1.3 μM, respectively. Minimal structural optimization of **8** resulted in compounds **15**, **19** and **20** with promising improvement in the inhibitory activity (IC₅₀ = 0.3 - 0.6 μM). The unprecedented chemical structures of **6** and **8**, which are prone to further derivatization reveal a new and attractive field for the development of mPGES-1 inhibitors with potential anti-inflammatory and anticancer properties.

Introduction

The microsomal prostaglandin E₂ synthase-1 (mPGES-1) has been the object of extensive research for next generation anti-inflammatory drugs during the last two decades.^[1] mPGES-1 is an inducible terminal enzyme in the biosynthesis of PGE₂, which is the main mediator of acute and chronic inflammation, fever and pain (Figure 1).^[1a] After its first discovery by Jakobsson and co-workers,^[2] mPGES-1 has rapidly become an attractive target for pharmacological intervention with inflammation-related diseases, such as arthritis, atherosclerosis, neuro-degenerative diseases and cancer.^[1b, 3] The biosynthesis of PGE₂ is initiated by the liberation of arachidonic acid (AA) from membrane phospholipids by phospholipases A₂. Cyclooxygenases (COX-1/2) then convert free AA to PGH₂, which is the junction point for the biosynthesis of several structurally related PGs that are formed from PGH₂ by the action of their respective PG synthases. The PGs biosynthesized by these pathways include PGE₂, PGD₂, PGF_{2α},

PGI₂ (prostacyclin) and thromboxane A₂ (TXA₂).^[1a] The isomerization of PGH₂ to PGE₂ is mediated by PGE₂ synthases (PGES), which include three members such as cytosolic PGE₂ synthase (cPGES) and two microsomal PGE₂ synthases (mPGES-1 and mPGES-2) (Figure 1). While both cPGES and mPGES-2 are constitutively expressed in a variety of tissues, mPGES-1, which is functionally coupled with COX-2, is strongly up-regulated under inflammatory conditions.^[1a] Therefore, it is believed that selective inhibition of mPGES-1 would selectively interfere with the biosynthesis of pro-inflammatory PGE₂, while intervention with COX-1/2 by nonsteroidal anti-inflammatory drugs (NSAIDs, such as indomethacin or ibuprofen) prevents the production of all PGs. Hence, inhibition of mPGES-1 has been a development of a pharmacological strategy for next generation NSAIDs that allow selective interference with pro-inflammatory PGE₂, and is anticipated to overcome the common side effects (i.e. gastrointestinal and cardiovascular) observed with current NSAIDs due to suppression of homeostatic prostanoids.

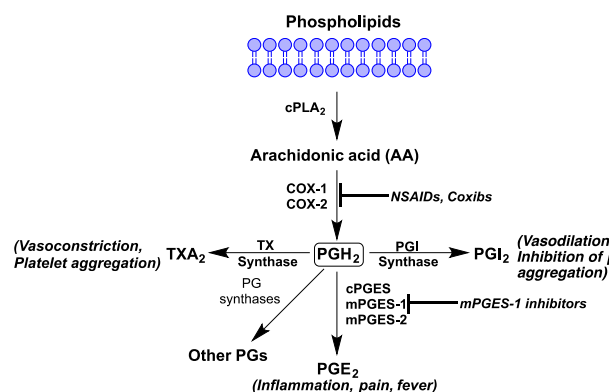


Figure 1. The Arachidonic acid pathway.

Figure 2 demonstrates several promising scaffolds that were developed as mPGES-1 inhibitors during the last decade.^[4] For example, indole-carboxylic acid derivatives, which was evolved from the structure of the 5-lipoxygenase-activating protein (FLAP)

FULL PAPER

inhibitor MK-886, effectively inhibit mPGES-1 activity *in vitro*.^[5] Other potent mPGES-1 inhibitors comprise various chemical scaffolds such as phenanthrene-imidazoles,^[6] 4-biarylimidazoles,^[7] tri-substituted urea derivatives,^[8] imidazoquinolines,^[9] dihydropyrimidines,^[10] and benzoxazole-piperidines.^[11] Although, these mPGES-1 inhibitors with distinct chemical classes have been identified, none has been proven clinically useful so far due to various problems (e.g. strong plasma protein binding and high lipophilicity) as reviewed elsewhere.^[4, 12] Up to now, only a single clinical trial with an mPGES-1 inhibitor (i.e. LY3023703 by Eli Lilly) has been reported,^[13] while a second compound from Glenmark Pharmaceuticals, namely GRC-27864, has recently entered phase I clinical development for the potential treatment of chronic inflammatory disorders such as osteoarthritis and rheumatoid arthritis (Clinical Trials Identifier: NCT02179645). To our knowledge, no structural information regarding both compounds has yet been disclosed. Therefore, developing new inhibitors of mPGES-1 with distinct scaffolds is a major challenge in anti-inflammatory drug development. Based on these considerations, we hereby report on the identification of new inhibitors of human mPGES-1 with various scaffolds through a multi-step virtual screening approach. We also show that these newly identified chemotypes are prone to further structural optimization for the development of potent mPGES-1 inhibitors as potential anti-inflammatory and anticancer agents.

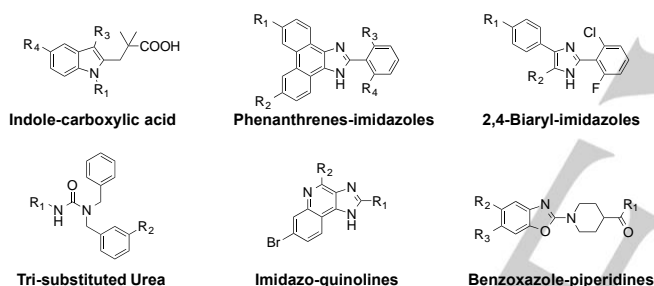


Figure 2. The main scaffolds of potent mPGES-1 inhibitors developed during the last decade.

Results and Discussion

Virtual screening (VS) and molecular docking are well-established computational methods that are appropriate to predict binding interactions of small molecules with experimental protein structures, and to retrieve putative small-molecule inhibitors from large chemical databases.^[14] However, some factors remain as challenging obstacles for obtaining a true prediction of the ligand-protein binding-affinity such as protein plasticity, water-mediated binding interactions, presence of structural water molecules in the active site and solvent entropy. Considering all these factors, we herein describe a multi-step VS protocol (Figure 3), which combines molecular docking, protein-ligand interactions profile, molecular dynamics (MD) simulations, and Molecular Mechanic–Poisson Boltzmann Surface Area (MM-PBSA) energy calculation in order to improve the virtual screening accuracy. Our final objective is to identify novel small-molecule mPGES-1 inhibitors devoid of cross-activity against COXs. The selection step in our protocol depended on preserving some key protein-ligand interactions as noticed in the four mPGES-1-inhibitor crystal

structures (4YL0, 4YL1, 4YL3, 4YK5) by investigating their stability using MD simulations followed by MM-PBSA calculations.

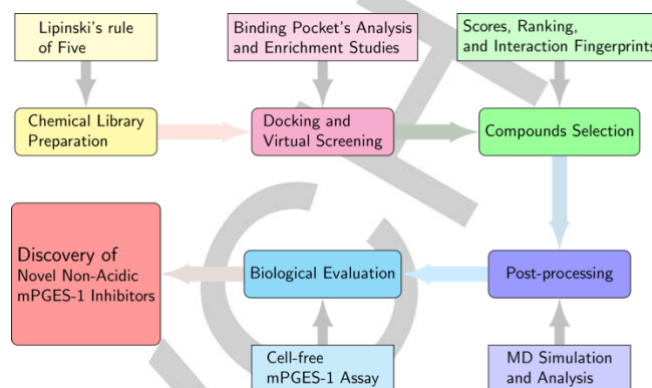


Figure 3. The workflow of the applied VS protocol.

Analysis of protein-ligand interactions in reported crystal structures of mPGES-1

The recent elucidation of the first crystal structure of mPGES-1 in an active form (PDB ID: 4AL1)^[15] was rapidly followed by elucidation of further high-resolution structures of human mPGES-1-inhibitor complexes (PDB ID: 4BMP, 4YK5, 4YL1, 4YL3 and 4YL0)^[16] to support the rational design of novel mPGES-1 inhibitors.^[17] With this aim, we retrospectively analyzed the reliability of a variety of available mPGES-1 crystal structures for use in our virtual screening study (Figure 4).

RES	P124	S127	V128	Y130	T131	R52	H53	F44	I32	N36	R38	L39	Y28
mon	(A)	(A)	(A)	(A)	(A)	(B)	(B)	(B)	(B)	(B)	(B)	(B)	(B)
4yl0	+	+(W)	+	-	-	-	+	+	-	-	+(W)	-	-
4yl1	+	-	+	-	+	+	+	+	-	-	+	+	-
4yl3	-	+	-	-	+	+	+	+	-	-	-	-	+
4yk5	-	-	-	+	+	+	+	-	+	-	-	+	+
Color code	+		+		+		+(W)		+		+		
Interaction	HYDROPHOBIC		IONIC		Hydrogen B.		Water Bridge		Halogen B.				

Figure 4. Important protein-ligand interactions for co-crystallized inhibitors in the published mPGES-1 crystal structures 4YL0, 4YL1, 4YL3, and 4YK5.

Careful analysis of binding modes of the co-crystallized inhibitors with mPGES-1 led to the recognition of a binding groove and important residues participating in the protein-ligand interactions. For example, X-ray crystal structures with PDB ID: 4YL0 and 4YL3 represent the mPGES-1 structures bound to a phenanthrene-imidazole derivative (MF-63) and a brominated biaryl-imidazole derivative, respectively (see Figure S1A-B for chemical structures). Both inhibitors bind between the two mPGES-1 monomers A and B, and more precisely, between two helical turns of α -4 from monomer A and α -1 from monomer B.^[15, 18] By examining the binding interactions, we mostly noticed strong hydrogen bonds in the more polar region close to residues S127 (from monomer A), H53 and R52 (from monomer B), while aromatic rings extended inside both the deep hydrophobic groove and binding groove above the co-substrate glutathione (GSH). Therefore, strong hydrophobic interactions are made with different residues such as A123 and S127 side chains (monomer

FULL PAPER

A) and R38, L39, F44, D49, H53, and R53 side chains (monomer B) (Figure 4).

In the case of MF63 (Figure S1A) in the crystal structure 4YL0, one of the imidazole's nitrogens contributes also to a hydrogen bond with H53, while the other may be involved either with hydrogen bond to GSH or via a bridge of water molecules connected with one of the ligand's cyanide groups (Figure 5A). The planar aromatic tetracycle is involved with multiple hydrophobic interactions with residues P124, S127 and V128 from monomer A. In case of the brominated biaryl-imidazole derivative (Figure S1B) in 4YL3, the bi-aryl hydrophobic tail interacts with P124, S127, V128, T131, L132 and L135 from monomer A (Figure 5B). In both structures, water molecules mediate protein-ligand interactions in order to fill distances and satisfy hydrogen bond's donors/acceptors in both the ligand and

the receptor (Figure 4 and 5).^[15-16] Other X-ray crystal structures (PDB ID: 4YK5 and 4YL1) have captured the binding of two indole-carboxylic acid derivatives (Figure S1C-D) to mPGES-1, showing double salt bridges between the inhibitor's carboxylate groups and the side chain of R52 from monomer B (Figure 4, Figure S2). In both structures, bridging water assists in mediating another interaction between the carboxylate and the neighboring residue H53. The aromatic ring, attached to the indole's nitrogen, extends in the binding groove above GSH, making hydrophobic interactions with the side chains of R38, L39, and F44 (from monomer B) and also with GSH. The fluorinated biaryl extension goes down the hydrophobic binding pocket making strong hydrophobic interaction with V128, Y130, and T131 (from monomer A) and on the other side with Y28 and I32 (from monomer B) (Figure S2, Figure 4).

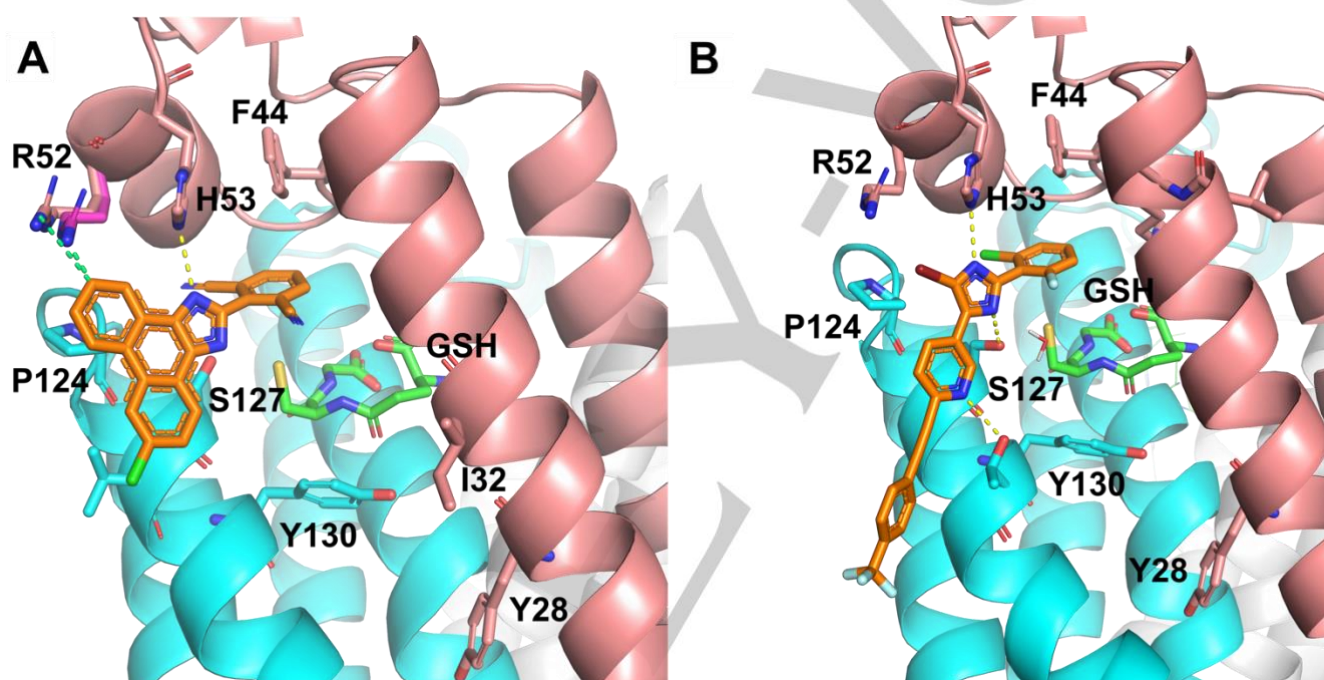


Figure 5. X-ray binding mode analysis of A) the phenanthrene-imidazole derivative (MF-63, Figure S1A) inside the binding pocket of mPGES-1 (PDB ID: 4YL0) between two monomers; Monomer A is shown in blue, while monomer B is shown in pink; the residue R52 from 4YL0 (in pink) is superimposed on the same residue from 4YL3 (the side chain in magenta) in order to show the difference of the side-chain conformation. B) The biaryl-imidazole derivative (Figure S1B) inside the binding pocket of mPGES-1 (PDB ID: 4YL3).

Molecular docking and enrichment studies

We tested the reliability of the Glide docking program (Schrödinger suite 2016) in order to analyze if the observed binding modes of inhibitor ligands in mPGES-1 crystal complexes (PDB ID: 4YK5, 4YL0, 4YL1, and 4YL3) were reproducible by docking experiments using the respective protein structures.^[16] All crystal ligands were successfully docked inside their respective crystal structures with low root-mean-square deviation (RMSD; 0 to 0.5 Å) to confirm the applicability of molecular docking experiments (Table S1 in Supplementary Information). However, the cross-docking of these four inhibitors in other crystal structures did not always produce the correct binding modes due to the distinct conformations of some flexible residues in different crystal structures. For example, Arg52 (R52) adopts different orientations in order to make the optimal hydrogen bonds network

between the specific enzyme structure and its respective ligand. The phenanthrene-imidazole ligand (MF63; Figure S1A) in 4YL0 with its voluminous aromatic tetracycle skeleton forces R52 to shift 1.15 Å outwards as compared to the same residue in structures 4YL3 and 4YL1 (Figure 5A). Consequently, docking programs may fail to dock phenanthrene-imidazole derivatives correctly to other crystal structures (4YK5, 4YL1, and 4YL3) due to a steric clash between the phenanthrene-imidazole ring and the R52, which would prevent the observed binding mode in the crystal structure 4YL0. Similarly, the indole-carboxylic acid derivative in structure 4YL1 shows a similar sensitivity for the right orientation of R52 in order to establish the salt bridge interactions. As a consequence, the correct binding mode of co-crystallized inhibitor in 4YL1 (Cmpd. 3 in Figure S1D) in different crystal structures was not always the top-scored solution but it appeared

FULL PAPER

as the second or third-ranked docking solution (Table S1 in the Supplementary Information).

Enrichment can be generally assessed by the number of active compounds detected at a given percent of the decoy set (presumed non-binding molecules) by score-ranked poses. Enrichment was calculated at 5%, 10%, and 20% of the ranked docked decoys by applying Glide SP score for ranking (Table 2). Another enrichment metrics, which was also estimated for the enrichment studies, includes the area under the accumulation curve (AUAC), and the area under the receiver operating characteristic (ROC) curve. The area under the ROC curve generally represents the inherent capability of the docking protocol and the used crystal structure to discriminate between the actives on one hand, and the inactives and the set of decoy molecules on the other hand. The results for 4YL0 structure indicate that 47.6% of the actives are retrieved when 20% of the decoys are captured (Figure S3). That yields the highest enrichment metrics for 4YL0 structure having area under the ROC curve as 0.75, while the area under the ROC curve for structures 4YL3, 4YL1, and 4YK5 is 0.67, 0.64 and 0.63, respectively. This difference in the performance can be simply explained by the incorrect docking of the highly active phenanthrene-imidazole derivatives in both structures 4YL3 and 4YK5 as pointed out earlier.

Table 1. Enrichment metrics for glide docking of mPGES-1 inhibitors together with 1000 decoy compounds from SCHROEDINGER's decoys set.

Enrichment [1000 Decoys + Inactives (IC ₅₀ ≥ 5 μM)]	5% Decoys	10% Decoys	20% Decoys	AUAC	ROC
4YL0	16.1	31.2	47.6	0.72	0.75
4YL3	14.35	23.7	33.7	0.63	0.67
4YK5	10.45	18.34	28.3	0.60	0.63
4YL1	11.63	19.84	29.58	0.61	0.64

The virtual screening work-flow

The general applied VS protocol includes several steps that are summarized in Figure 3. In the first step, a proper chemical library was generated starting from the MolPort screening library with adequate geometries, ionization states, conformations, and tautomers using the LigPrep module in SCHROEDINGER 2016 suite. In the early step, the Lipinski's rules of five (RO5) were applied as filter in order to establish a library with compounds displaying high drug-likeness.^[19] Both crystal structures (4YL0 and 4YL3) were used in the VS study in order to take two different conformations of the R52 side chain into account. In the first structure-based VS tour, all drug-like compounds retrieved from MolPort database (about 5 mio compounds) were subjected to molecular docking to the mPGES-1 binding site using the crystal structure 4YL0. Later, the top scored compounds (40,000 compounds) were docked again into another crystal structure, namely 4YL3, in order to consider the two different conformations of the R52. Then, a first diversity-based selection protocol was applied to the docking poses that survived using both structural MACCS- and pharmacophore-based fingerprints application in SCHROEDINGER's canvas to obtain 1000 docking complexes

RES	P124	R126	S127	Y130	T131	Q134	R52	H53	D49	F44	I32	L39	Y28
mon	(A)	(A)	(A)	(A)	(A)	(A)	(B)	(B)	(B)	(B)	(B)	(B)	(B)
1	+	-	+	(pi)+	-	+	-	+	-	-	-	-	-
2	+	-	+	(pi)+	+	+	-	+	-	+	-	-	+
3	-	-	+	+	+	+	-	+	+	+	+	+	-
4	-	-	+	+	+	+	+	+	-	-	-	+	-
5	+	-	+	+	+	+	-	+	-	+	+	+	+
6	+	-	+	+	+	+	-	+	+	+	+	+	-
7	-	-	+	(pi)+	+	+	+	+	+	+	+	+	+
8	-	-	+	+	+	+	-	+	+	+	+	-	-
9	-	-	+	+	+	-	-	+	+	(pi)+	+	-	+
10	+	-	+	+	+	+	-	+	+	+	+	+	-
15	-	-	+	+	+	-	-	+	-	+	+	+	-
19	-	+	+	(pi)+	+	-	-	+	-	(pi)+	+	+	-
20	-	+	+	(pi)+	+	-	-	+	-	(pi)+	+	+	-

Color code	+	+	+	(pi)+
Interaction type	HYDROPHOBIC	IONIC	Hydrogen Bond	π-π

Figure 6. The protein-ligand interactions for the VS-hits and compound 8 derivatives docked inside mPGES-1 crystal structure 4YL3.

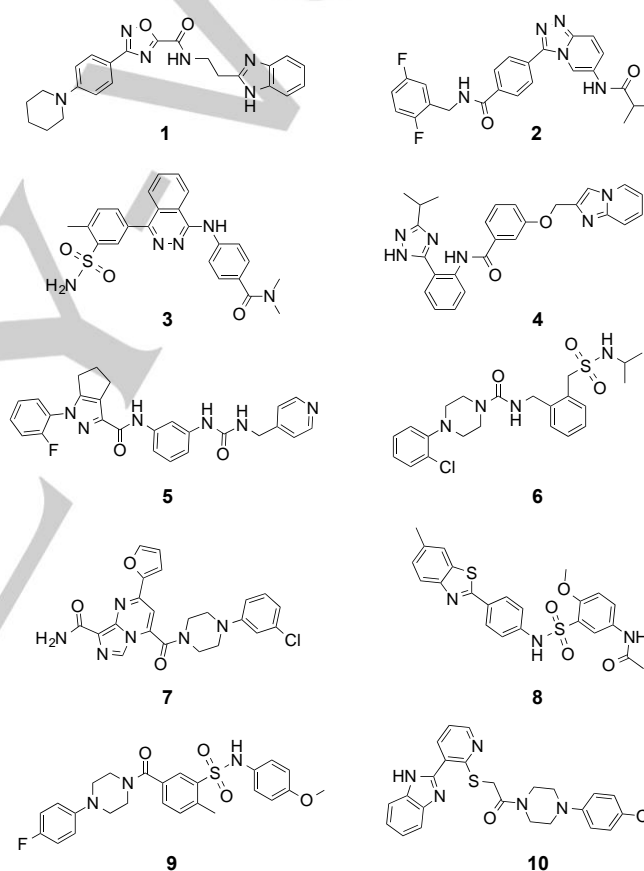


Figure 7. Chemical structures of the selected VS hits. Among them, the two structures 6 and 8 were identified as promising mPGES-1 inhibitors in cell-free activity assays with IC₅₀ = 1.2 and 1.3 μM respectively.

with chemically diverse scaffolds. In the next step, the open-source software PLIP (protein-ligand interaction profiler) was used to process the final 1000 docking complexes for characterization of the most diverse protein-ligand interaction pattern.^[20] As a result, a subset of 49 hits was selected based on diversity observed in protein-ligand interaction profiles as well as in chemical structures. Finally, ten candidates were 'cherry-picked' from this subset based on chemical intuition, literature knowledge considering the geometrical and pharmacophoric features (i.e.,

FULL PAPER

non-acidic features) and similarity to the protein-interaction profile of the mPGES-1-co-crystallized inhibitors (Figures 6 and 7). All selected candidates were chosen to have good similarity (Tanimoto index > 0.75) to the protein-interaction profile of the mPGES-1-co-crystallized inhibitors, which provide one hydrogen bond at least to residues of H53, R52 and S127, and at least two hydrophobic interactions with the set of residues comprising F44, P124, Y130, L39 or Y28 as presented in Figure 6. Accordingly, to

further investigate the stability of the binding modes of selected compounds to mPGES-1 considering potential ligand-induced conformational changes, we performed MD simulations (20 ns) using the 3D structure of mPGES-1 (PDB ID: 4YL3 in complex with these docked ligands), followed by MM-PBSA energy decomposition per residue as will be discussed later.

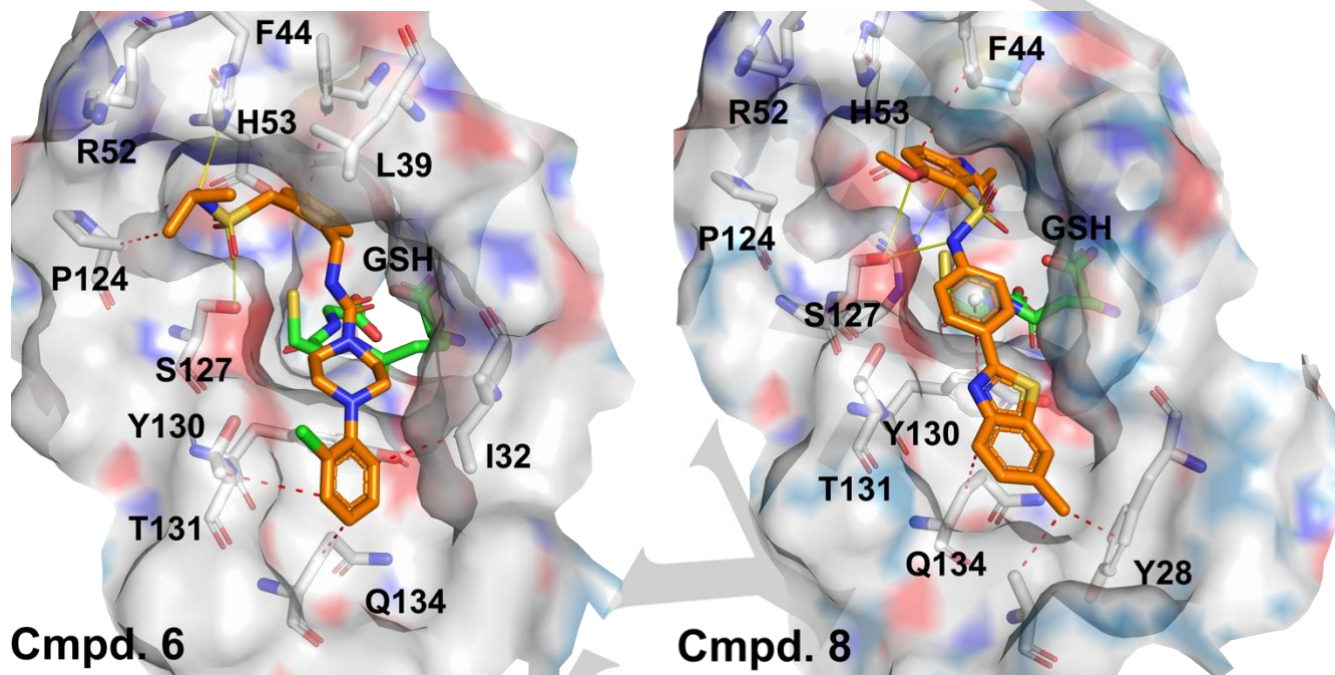


Figure 8. The suggested binding mode of the identified mPGES-1 inhibitors **6** and **8**, as docked inside the putative binding pocket of mPGES-1 (PDB ID: 4YL3). Hydrogen bonds are shown in yellow, while the pi-pi stacking and hydrophobic interactions are represented by red dashes.

MD simulations: Analysis, MM-PBSA calculation, and energy decomposition

MD simulations were performed on the selected VS hits in order to prove the stability of the suggested binding mode and to examine the dynamic variations of the ligand-protein interactions. The time series of the RMSD of the docking complexes were under 2.6 Å over 20 ns of MD simulation, and under 0.5 Å for the simulated ligands in the putative binding pocket. To further investigate the protein-ligand interactions over the MD trajectory, the MM-PBSA method was used to estimate the binding energy and to perform energy decomposition by residue (using *g_mmpbsa* tool)^[21], although an efficient algorithm for calculating the entropy term is still lacking.^[22] Additionally, the presence of the bilayer membrane in the case of membrane proteins would make the exact description of desolvation and calculation of entropy term even more complex. Therefore, the application of MM-PBSA binding energy calculation was not intended to reproduce the exact binding free energy, but to estimate the energetic contribution of the key protein residues to the protein-ligand binding. The calculated free binding energies of the native co-crystallized ligands in two mPGES-1 crystal structures (4YL0 and 4YL3) as well as three of the selected VS compounds (**6**, **7**, and **8**) are listed in Table S3, with the contributions from vdW, electrostatic interaction, polar desolvation, and apolar desolvation energy terms using MM-PBSA method.

The decomposition of the binding energy of the mPGES-1/VS-hits complexes showed a significant contribution of aforementioned key residues (S127, R126, H53, and R52) in establishing a hydrogen bonds' network between the ligand and the protein. The most recognized hydrophobic residues in the decomposition analysis appeared to be P124, A123, F44, L39, and Y130. The list of key residues can be extended to T131, Q134, I32, and Y28. The binding of **6**, as an example, appeared to be mostly driven by interactions with several hydrophobic residues such as P124, L39, and I32, and A123 while the electrostatic and polar interactions were contributed mainly by S127, R52, R126, and Q134. In the case of **8**, the hydrophobic interactions were contributed mainly by Y130, P124, L39, and I32, while polar interactions were mainly made with H53, R38, and S127. Moreover, the analysis of MD snapshots with an explicit solvent model can also show water-mediated interactions between the studied ligands (from the VS selected compounds) and some key residues such as R53, H53, or S127. For both **6** and **8**, we observed an optimal orientation of one aromatic ring close to the residues F44 and L39, while other aromatic rings interact with other hydrophobic residues, e.g., Y28, Y130, T131, and I32 (Figure 8).

Biological evaluation and SAR

The mPGES-1 inhibitory activity of the acquired compounds was assessed using a well-established cell-free assay based on

FULL PAPER

incubation of microsomes from IL-1 β -activated human A549 cells, which strongly express mPGES-1, with 20 μ M PGH₂ as substrate.^[23] The mPGES-1 inhibitor MK886 was used as a reference compound (IC₅₀ = 1.6 μ M, not shown). Among the tested compounds (1 and 10 μ M, final concentration), **6** and **8** effectively inhibited the activity of mPGES-1 while the other compounds were less efficient (Table 2). More detailed concentration-response analysis revealed the IC₅₀ values of 1.2 \pm 0.2 μ M for **6** and 1.3 \pm 0.4 μ M for **8** (Table 3). Because many mPGES-1 inhibitors tend to inhibit also COX-1 (including MK886),^[3b, 24] we investigated the two hit compounds for COX-1 inhibition. However, **6** and **8** displayed no inhibitory effectiveness against COX-1 activity in a cell-based assay using human platelets up to 10 μ M (Figure S4).

Table 2. Inhibitory effects of newly identified hit compounds **1** - **10** on PGE₂ formation at concentrations of 1 μ M and 10 μ M using the IL-1 β -activated A549 cells expressing mPGES-1 and 20 μ M PGH₂ as substrate.

Cmpd.	Remaining mPGES-1 activity ^[a] in % of control at	
	1 μ M	10 μ M
1	86.7 \pm 4.5	63.1 \pm 3.0
2	88.6 \pm 1.2	79.8 \pm 2.5
3	99.1 \pm 4.3	83.8 \pm 2.9
4	73.4 \pm 2.3	67.8 \pm 1.9
5	90.2 \pm 5.1	74.9 \pm 9.7
6	52.9 \pm 1.0	16.2 \pm 1.0
7	83.4 \pm 3.6	60.9 \pm 1.5
8	54.9 \pm 2.0	35.2 \pm 1.8
9	80.9 \pm 3.3	65.5 \pm 2.2
10	83.0 \pm 2.0	77.5 \pm 1.2

[a] Data are given as means \pm SEM, n=3.

Table 3. In vitro inhibitory activities of newly identified mPGES-1 inhibitors under cell-free conditions.

Cmpd.	IC ₅₀ (μ M) ^[a]	Cmpd.	IC ₅₀ (μ M)
6	1.2 \pm 0.2	16	5.0 \pm 0.4
8	1.3 \pm 0.4	17	>10
12	2.3 \pm 1.3	18	1.4 \pm 0.7
14	7.0 \pm 2.1	19	0.6 \pm 0.2
15	0.6 \pm 0.1	20	0.3 \pm 0.1

[a] The IC₅₀ values are given as mean \pm SEM of n = 3-4 determinations.

Based on the VS results obtained, we selected **8** for further structural optimization to deduce preliminary structure-activity relationships in a small series of synthesized (**12**, **14**-**16**, see supporting information for synthesis) or commercially available

(**17**-**20**) compounds (Figure 9). We first focused on the heterocyclic ring occupying the deep hydrophobic binding cavity and obtained the closely related analogues having benzothiazole (**12**) and benzoxazole (**14**) rings. Results from the biological assessment of mPGES-1 inhibition by **12** and **14** indicated that **12** with a benzothiazole ring (IC₅₀ = 2.3 μ M) was superior to the benzoxazole (**14**, IC₅₀ = 7 μ M) counterpart (Table 3). Next, we investigated the position of the 3-acetylamino function and obtained the 4-acetylamino congeners **15**-**17** with the hypothesis of the gain of further favorable contacts with amino acids R52, H53 and F44 at the upper part of the substrate binding cavity. As seen from table 4, **15** with a benzothiazole ring as compared to **16** and **17** with benzoxazole and benzimidazole, respectively, resulted in significant inhibition of mPGES-1 activity (IC₅₀ = 0.6, 5 and >10 μ M, respectively). Removal of the acetylamino function in the benzothiazole series (**18**) caused a small decrease in the inhibitory activity (IC₅₀ = 1.4 μ M). At this point, in particular, the presence of the benzothiazole ring guaranteed the most potent mPGES-1 inhibition, and additionally suggested that the presence of more appropriate polar aromatic functions at the upper end of the molecule might significantly contribute to the inhibitory activity by establishing additional polar and π - π interactions with amino acids at the cytosolic entrance (i.e., R52, H53, R126, F44). Therefore, we searched the MolPort database for closely related congeners leading to commercially available **19** and **20** with benzofurazan and benzoxazolone rings, respectively, as a replacement of the 4-acetylamino phenyl part in compound **15**. As expected, both compounds profoundly inhibited mPGES-1 activity with IC₅₀ values of 0.6 and 0.3 μ M, thereby corroborating our hypothesis (Table 3).

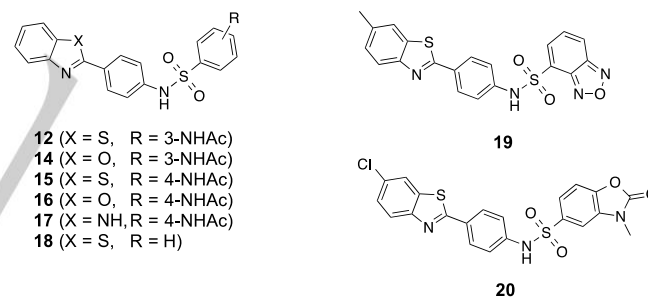


Figure 9. Chemical structures of analogues of compound **8**.

Docking studies and molecular dynamic (MD) simulations

To provide further insights into the interaction of **15**, **19**, and **20** with mPGES-1, we performed docking studies in combination with MD simulations (20 ns) using the mPGES-1 crystal structure (PDB code: 4YL3). According to the docking and MD simulations performed on the inhibitors/protein complexes inside lipid bilayer (POPC model), we clearly observed stable π - π interactions between the benzothiazole aromatic rings of all three compounds and the residue Y130 from mPGES-1 structure (Figure 10). Moreover, the enhanced protein-ligand interactions are mainly noticed inside the catalytic pocket above GSH where **15**, **19** and **20** interact with residues H53, D49, R126 or S127 by hydrogen bonds, while the aromatic rings of **19** and **20** (benzofurazan in **19** and benzoxazolone in **20**) establish additional π - π stacking or charge- π interactions with the residues F44 or R126, respectively. MD studies of both **19** and **20** offer an overview of stable hydrogen

FULL PAPER

bond with H53 (for **19**) or S127 (for **20**), stabilized by one or two additional hydrogen bonds with R126 (for **19**) or D49 (for **20**). Moreover, both compounds were able to maintain stable π - π

stacking with at least two of the aromatic residues of the binding pocket such as Y28 and Y130 (for **19**), or Y130 and F44 (for **20**).

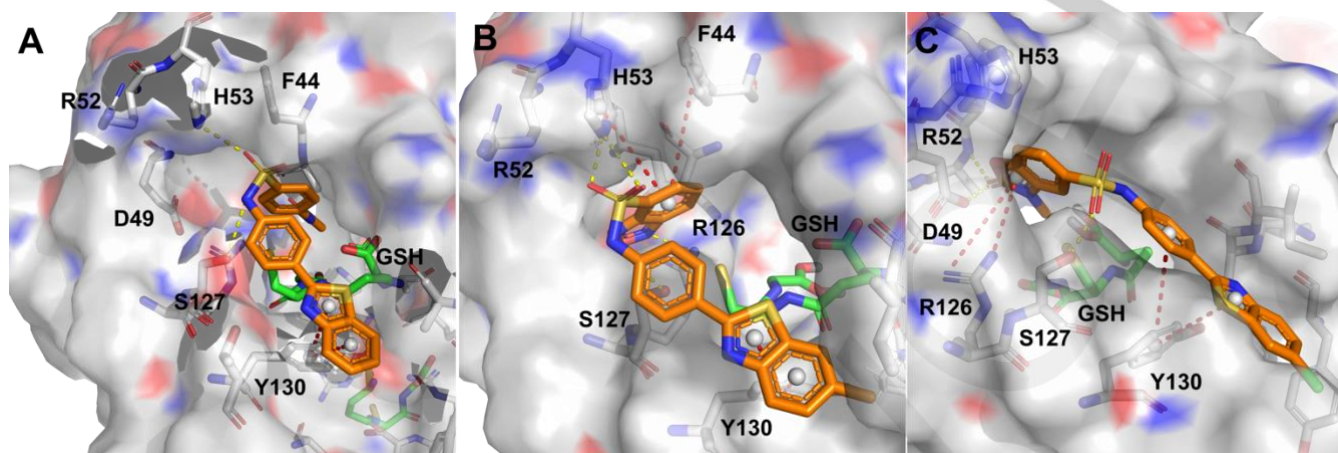


Figure 10. Binding mode analysis of **15** (A), **19** (B) and **20** (C) during interaction with mPGES-1 (PDB code: 4YL3) considering membrane residues. Main interactions are represented schematically considering MD simulations in the time window 0-20 ns. Hydrogen bonds are represented by yellow dashes, while the pi-pi stacking interactions are represented by red dashes.

Conclusions

There is currently a strong interest in the development of mPGES-1 inhibitors because of their promising potential as safer and effective therapeutics in inflammatory diseases. In recent years, we see an increase in the number of VS studies for the discovery of novel mPGES-1 inhibitors, which utilize ligand- and structure-based approaches with distinct methodologies. For example, Lauro et al. recently reported the structure-based virtual fragment growing optimization for the development of new mPGES-1 inhibitors leading to sulfonamide-based mPGES-1 inhibitors.^[17a] In another recent study, Rörsch et al. demonstrated that a multistep VS methodology on a rather small library of compounds (360,169 compounds from Asinex) can be successfully used for identification of non-acidic mPGES-1 inhibitors.^[25] Additional studies from Schuster lab showed that urea-based virtual screening hits, identified from 450,000 structures of NCI and Specs databases, would be a good starting point for further development of mPGES-1 inhibitors.^[26] Apart from others, He et al. identified novel mPGES-1 inhibitor structures in nM range by applying a three-step VS scheme combining both docking and molecular mapping on the Specs library of 197,211 compounds.^[27] Based on the aforementioned potential of VS approaches, we hereby have implemented a rapid VS study on a large number of compounds from vendor libraries for identification of novel mPGES-1 inhibitor chemotypes using the recent mPGES-1 structures co-crystallized with some distinct and potent mPGES-1 inhibitors. The protocol starts with docking of a huge screening library comprising 5 million drug-like compounds, followed by fingerprints-based clustering and diversity-based selection. Subsequent steps were performed to ensure the protein-ligand interaction fingerprints as observed in four crystal structures. Out of ten candidates that were tested, the sulfonamide-containing compounds **6** and **8** were identified as potent suppressors of PGE₂ biosynthesis without inhibiting COX-

1 activity. Depending on the study of various crystal structures of mPGES-1, it appears that the binding to the region around glutathione is quite important in order to block the access of the substrate PGH₂ in which the hit compounds **6** and **8** efficiently occupy. In addition, starting from **8**, we have performed a preliminary SAR study with a small series of closely related structures, and obtained **15**, **19** and **20** with an improved activity (IC₅₀ = 0.3 - 0.6 μ M). Computational data demonstrated that the more potent benzothiazole derivatives **15**, **19** and **20** were able to gain several interactions at the upper part of the substrate binding site without affecting the original binding mode of **8**. As a result, our protocol was proven successful for identifying two promising scaffolds that warrant further chemical development as non-acidic mPGES-1 inhibitors.

Experimental Section

Computational studies

Docking: Crystal structures preparation and enrichment studies

Four scaffolds of active mPGES-1 inhibitors were presented in four recently published crystal structures (PDB ID: 4YK5, 4YL0, 4YL1 and 4YL3) in which 4YK5 and 4YL0 are in complex with two biaryl-indoles; 4YL0 is in complex with phenanthrene imidazole (MF63), while the inhibitor structure in 4YL3 is a biaryl-imidazole (Compd. 3 in Fig. S1B)^[16] The PDB coordinates of the X-ray complexes 4YK5, 4YL0, 4YL1 and 4YL3 were obtained from the protein data bank website as a biological assembly of three identical chains. The biological assembly files were imported into Maestro software and merged in order to obtain the homotrimer of mPGES-1 structures. Charges and bond orders were assigned, hydrogens were added to the heavy atoms, and all waters were deleted. Docking studies were carried out in one of the ligand binding sites of the crystal structures 4YK5, 4YL0, and 4YL3. Glide energy grids were calculated inside a box centered on the co-crystallized ligand's centroid with dimensions of 15 Å.^[28]

FULL PAPER

The Schrödinger decoy set, which consists of 1000 drug-like compounds with an average molecular weight of 400 Daltons, was used to validate the docking protocol and the suitability of the used crystal structures.^[29] The enrichment studies were carried out by docking ChEMBL compounds with reported bioactivity against mPGES-1 (from ChEMBL 21 database^[30]) after seeding them with Schrödinger decoys set. We considered all reported structures with K_i or IC_{50} less than 1 μ M as part of the mPGES-1 active inhibitors (303 structures), while the compounds with $IC_{50} > 5 \mu$ M as a set of inactives (412 structures). The interactions between the protein with the ligand in the crystal structures were characterized using the open-source program 'protein–ligand interaction profiler' (PLIP).^[20]

Virtual screening: Library preparation, docking and filtration

MolPort's screening library is a well-maintained database of commercially available screening compounds integrated with ZINC library, and synchronized with the most warehouse databases of prominent chemical companies. The MolPort screening library, which contains a collection of 6.5 million synthetic compounds from 21 chemical vendors (as downloaded in March 2016), has been imported into Canvas software^[31] in order to build the 3D coordinates and calculate the physio-chemical properties. The imported structures have been filtered according to Lipinski's rules of five (log P in the range -0.4 to $+5.6$, molecular weight in the range 150 to 500, polar surface area (PSA) ≤ 140 , hydrogen bonds donors ≤ 5 , hydrogen bonds acceptors ≤ 10).^[19] The drug-like selected 5 million chemical compounds have been prepared using LigPrep^[32] in order to use for generation of all the possible isomers and tautomers, lowest energy ring conformations, and also all possible ionization states (protonation/deprotonation) at $Ph = 7.0 \pm 1$ using the Epik software.^[33] The generated isomers/tautomers were docked using GLIDE^[34] in one of the binding pockets of the crystal 4YL0 inside the generated grid and Glide SP score as the fitness function. The top 40,000 docking solutions with highest Glide scores were later docked again inside the crystal structure of 4YL3 in order to perform ensemble docking. From both docking results, we have selected the top-scored 10,000 docking solutions in order to select a list of virtual screening hits. The selected 10,000 docking solution were imported in Canvas software^[35] in order to generate two kinds of fingerprints such as structure-based and pharmacophore-based fingerprints. In the final step, a clustering and diversity-based selection was applied using Tanimoto similarity metric in order to choose 1,000 unique scaffolds from the list of the top ten thousand docking solutions, and later the protein–ligand interactions were applied on the chosen docking complexes also using the open-source 'protein–ligand interaction profiler' (PLIP) as a stand-alone program.^[20]

Molecular dynamics (MD) simulation

In order to obtain the coordinates of the mPGES-1 crystal structures (PDB ID: 4YL0 and 4YL3) immersed in bi-layer of POPC (monounsaturated 1-palmitoyl-2-oleoyl-sn-glycero-3-phosphocholine) membrane, the MD system preparation in SCHRODINGER suite 2016 was used,^[36] and the generated system was later compared to the membrane location in OPM database (4YL3.pdb is available in OPM).^[37] The MD simulation was performed using the open-source software Gromacs 5.1^[38] as the protein atoms were parameterized by the amber99sb force field, while the LIPID14 amber's special force field for lipids was used for the lipid bi-layer membrane.^[39] The docked ligand/inhibitor was parameterized by GAFF force field using amber14's antechamber tool,^[40] and converted to Gromacs coordination and topology format using ACPYPE software.^[41] For the preparation for the molecular dynamics system, the protein was centered inside a cubic box with dimensions 9.50, 9.50 and 8.50 nm. TIP3P model of water molecules has been used when the system was solvated on both sides of the membrane. The system was neutralized using a mixture of the chloride Cl^- and sodium Na^+ ions to provide 100 mM salt concentration. After energy minimization, a short NVT equilibrium was applied for 100 ps (50,000 steps with a 2 fs time-step) with position restraints applied on the protein's backbone. Temperature coupling is performed on four groups of the simulated system: Protein, lipids (POPC),

ligand, and water-ions using V-rescale algorithm (a modified Brendesen thermostat) in order to reach a temperature of 310 K. Leap-frog integrator was used with linear constraint solver (LINCS) algorithm applied to all bonds. The cutoff for short-range electrostatics and van der Waals interactions was 1.2-nm. The second phase of NPT equilibrium was performed for 500 ps (250,000 steps) using similar conditions like the previous NVT equilibrium (Position restraints and short-range interactions' cutoff), except using Nose-Hoover thermostat for temperature coupling at 310 K. The temperature coupling was also applied to the exact four groups of the system. After the two equilibration phases, a production simulation is performed with the same parameters as NPT run but without position restraints.

MM-PBSA calculation

For the calculation of MM-PBSA energy, 50 snapshots were extracted from the last nanosecond of 20 nanoseconds MD trajectory, which means using the interval of 20 ps from the production trajectory between 19 to 20 ns. The program `g_mmpbsa`^[21b] was used for estimating the binding free energies, and later to perform the energy decomposition in order to obtain the contribution per residue to the binding energy. The energy components (ΔE_{MM} , ΔG_{P-SOLV} and $\Delta G_{NP-SOLV}$) for individual atoms were calculated in the bound and the unbound form, and subsequently their contribution to the binding energy of residue x , abbreviated as $\Delta R_{BE}(x)$ is calculated. ΔE_{MM} is the average molecular mechanics potential energy in vacuum, while ΔG_{SOLV} is the free energy of solvation and is divided into polar term ΔG_{P-SOLV} non-polar term $\Delta G_{NP-SOLV}$. The calculation was performed depending on the solvent accessible surface area (SASA) model, which assumes linear correlation between SASA and the non-polar solvation energy. As the entropy contribution is not included in this protocol, the calculated energy is not expected to be comparable to the absolute binding energy, but to relative binding energy. In MM-PBSA, the binding energy is evaluated according to the equation below:

$$\Delta G_{bind} = \Delta E_{MM} + \Delta G_{P-SOLV} + \Delta G_{NP-SOLV} - T \cdot \Delta S = \Delta E_{VDW} + \Delta E_{ELE} + \Delta G_{P-SOLV} + \Delta G_{NP-SOLV} - T \cdot \Delta S$$

The Entropy term ($-T \cdot \Delta S$) wasn't calculated during this study. ΔG_{P-SOLV} is the polar solvation contribution calculated by solving the non-linear Poisson-Boltzmann (PB) equation using the open-source program APBS.^[42] The values for the solute and solvent dielectric constants were chosen to be 7 and 80, respectively.^[43] The non-polar solvation free energy, $\Delta G_{NP-SOLV}$ was estimated by the solvent accessible surface area (SASA) using a water probe radius of 1.4 Å, according to the equation $\Delta G_{NP-SOLV} = \gamma \cdot SASA + b$ where the constants γ and b were set to 0.022 kJ/mol/Å² and 3.84 kJ/mol, respectively.^[21b]

Biological assays

Determination of mPGES-1 activity

Microsomal preparations of A549 cells expressing mPGES-1 were prepared as previously described.^[23] In brief, A549 cells were cultivated in DMEM medium containing FCS (2%) and IL-1 β (2 ng/mL) for 72 h (37 °C, 5% CO₂). Cells were harvested and resuspended in homogenization buffer consisting of potassium phosphate (0.1 M, pH 7.4), phenylmethanesulfonyl fluoride (1 mM), soybean trypsin inhibitor (60 μ g/mL), leupeptin (1 μ g/mL), glutathione (2.5 mM), and sucrose (250 mM). After shock-freezing of the cells in liquid nitrogen, sonication (3x20 s), and differential centrifugation at 10,000xg (10 min, 4 °C) and 174,000xg (60 min, 4 °C), the pellets were resuspended in homogenization buffer. Microsomes were diluted in potassium phosphate buffer (0.1 M, pH 7.4) with glutathione (2 mM) and pre-incubated with the test compounds or vehicle (0.1% DMSO) on ice for 15 min. After stimulation for 1 min at 4 °C with 20 μ M PGH₂ as substrate, the reaction was terminated by addition of stop solution containing FeCl₃ (40 mM), citric acid (80 mM), and 11 β -PGE₂ (10 μ M, as internal standard) and analyzed for PGE₂ by RP-HPLC as reported before.^[23]

FULL PAPER

Acknowledgements

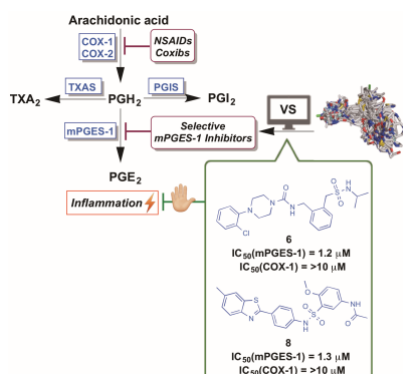
We would like to acknowledge the Turkish Academy of Sciences (TÜBA) and the Deutsche Forschungsgemeinschaft SFB1278 "Polytarget" for financial support. Suhaib Shekfeh acknowledges the Scientific and Technological Research Council of Turkey (TUBITAK)-BIDEB 2221 Fellowships for Visiting Scientists for the fellowship. One of the GPUs used in this study was a donation from Nvidia Corporation.

Keywords: Microsomal prostaglandin E₂ synthase-1 • prostaglandin • virtual screening • docking • inflammation

References:

- [1] a) C. D. Funk, *Science* **2001**, *294*, 1871-1875; b) B. Samuelsson, R. Morgenstern, P. J. Jakobsson, *Pharmacol Rev* **2007**, *59*, 207-224.
- [2] P. J. Jakobsson, S. Thoren, R. Morgenstern, B. Samuelsson, *Proc Natl Acad Sci U S A* **1999**, *96*, 7220-7225.
- [3] a) I. Gomez, N. Foudil, D. Longrois, X. Norel, *Prostaglandins Leukot Essent Fatty Acids* **2013**, *89*, 55-63; b) A. Koeberle, O. Werz, *Biochem Pharmacol* **2015**, *98*, 1-15; c) K. Larsson, P. J. Jakobsson, *Prostaglandins Other Lipid Mediat* **2015**, *120*, 161-165.
- [4] H. H. Chang, E. J. Meuliet, *Future Med Chem* **2011**, *3*, 1909-1934.
- [5] D. Riendeau, R. Aspiotis, D. Ethier, Y. Gareau, E. L. Grimm, J. Guay, S. Guiral, H. Juteau, J. A. Mancini, N. Methot, J. Rubin, R. W. Friesen, *Bioorg Med Chem Lett* **2005**, *15*, 3352-3355.
- [6] a) B. Cote, L. Boulet, C. Brideau, D. Claveau, D. Ethier, R. Frenette, M. Gagnon, A. Giroux, J. Guay, S. Guiral, J. Mancini, E. Martins, F. Masse, N. Methot, D. Riendeau, J. Rubin, D. Xu, H. Yu, Y. Ducharme, R. W. Friesen, *Bioorg Med Chem Lett* **2007**, *17*, 6816-6820; b) A. Giroux, L. Boulet, C. Brideau, A. Chau, D. Claveau, B. Cote, D. Ethier, R. Frenette, M. Gagnon, J. Guay, S. Guiral, J. Mancini, E. Martins, F. Masse, N. Methot, D. Riendeau, J. Rubin, D. Xu, H. Yu, Y. Ducharme, R. W. Friesen, *Bioorg Med Chem Lett* **2009**, *19*, 5837-5841.
- [7] T. Y. Wu, H. Juteau, Y. Ducharme, R. W. Friesen, S. Guiral, L. Dufresne, H. Poirier, M. Salem, D. Riendeau, J. Mancini, C. Brideau, *Bioorg Med Chem Lett* **2010**, *20*, 6978-6982.
- [8] J. F. Chiasson, L. Boulet, C. Brideau, A. Chau, D. Claveau, B. Cote, D. Ethier, A. Giroux, J. Guay, S. Guiral, J. Mancini, F. Masse, N. Methot, D. Riendeau, P. Roy, J. Rubin, D. Xu, H. Yu, Y. Ducharme, R. W. Friesen, *Bioorg Med Chem Lett* **2011**, *21*, 1488-1492.
- [9] a) T. Shiro, K. Kakiguchi, H. Takahashi, H. Nagata, M. Tobe, *Bioorg Med Chem* **2013**, *21*, 2868-2878; b) T. Shiro, H. Takahashi, K. Kakiguchi, Y. Inoue, K. Masuda, H. Nagata, M. Tobe, *Bioorg Med Chem Lett* **2012**, *22*, 285-288.
- [10] G. Lauro, M. Strocchia, S. Terracciano, I. Bruno, K. Fischer, C. Pergola, O. Werz, R. Riccio, G. Bifulco, *Eur J Med Chem* **2014**, *80*, 407-415.
- [11] a) G. B. Arhancet, D. P. Walker, S. Metz, Y. M. Fobian, S. E. Heasley, J. S. Carter, J. R. Springer, D. E. Jones, M. J. Hayes, A. F. Shaffer, G. M. Jerome, M. T. Baratta, B. Zweifel, W. M. Moore, J. L. Masferrer, M. L. Vazquez, *Bioorg Med Chem Lett* **2013**, *23*, 1114-1119; b) D. P. Walker, G. B. Arhancet, H. F. Lu, S. E. Heasley, S. Metz, N. M. Kablaoui, F. M. Franco, C. E. Hanau, J. A. Scholten, J. R. Springer, Y. M. Fobian, J. S. Carter, L. Xing, S. Yang, A. F. Shaffer, G. M. Jerome, M. T. Baratta, W. M. Moore, M. L. Vazquez, *Bioorg Med Chem Lett* **2013**, *23*, 1120-1126.
- [12] A. Koeberle, S. A. Laufer, O. Werz, *J Med Chem* **2016**, *59*, 5970-5986.
- [13] Y. Jin, C. L. Smith, L. Hu, K. M. Campanale, R. Stoltz, L. G. Huffman, Jr., T. A. McNearney, X. Y. Yang, B. L. Ackermann, R. Dean, A. Regev, W. Landschulz, *Clin Pharmacol Ther* **2016**, *99*, 274-284.
- [14] C. McInnes, *Curr Opin Chem Biol* **2007**, *11*, 494-502.
- [15] T. Sjogren, J. Nord, M. Ek, P. Johansson, G. Liu, S. Geschwindner, *Proc Natl Acad Sci U S A* **2013**, *110*, 3806-3811.
- [16] J. G. Luz, S. Antonyamy, S. L. Kuklish, B. Condon, M. R. Lee, D. Allison, X. P. Yu, S. Chandrasekhar, R. Backer, A. Zhang, M. Russell, S. S. Chang, A. Harvey, A. V. Sloan, M. J. Fisher, *J Med Chem* **2015**, *58*, 4727-4737.
- [17] a) G. Lauro, P. Tortorella, A. Bertamino, C. Ostacolo, A. Koeberle, K. Fischer, I. Bruno, S. Terracciano, I. M. Gomez-Monterrey, M. Tauro, F. Loiodice, E. Novellino, R. Riccio, O. Werz, P. Campiglia, G. Bifulco, *ChemMedChem* **2016**, *11*, 612-619; b) M. A. Schiffler, S. Antonyamy, S. N. Bhattachar, K. M. Campanale, S. Chandrasekhar, B. Condon, P. V. Desai, M. J. Fisher, C. Groshong, A. Harvey, M. J. Hickey, N. E. Hughes, S. A. Jones, E. J. Kim, S. L. Kuklish, J. G. Luz, B. H. Norman, R. E. Rathmell, J. R. Rizzo, T. W. Seng, S. J. Thibodeaux, T. A. Woods, J. S. York, X. P. Yu, *J Med Chem* **2016**, *59*, 194-205; c) Z. Zhou, Y. Yuan, S. Zhou, K. Ding, F. Zheng, C. G. Zhan, *Bioorg Med Chem Lett* **2017**, *27*, 3739-3743.
- [18] D. Li, N. Howe, A. Dukkupati, S. T. Shah, B. D. Bax, C. Edge, A. Bridges, P. Hardwicke, O. M. Singh, G. Giblin, A. Pautsch, R. Pfau, G. Schnapp, M. Wang, V. Olieric, M. Caffrey, *Cryst Growth Des* **2014**, *14*, 2034-2047.
- [19] C. A. Lipinski, *J Pharmacol Toxicol Methods* **2000**, *44*, 235-249.
- [20] S. Salentin, S. Schreiber, V. J. Haupt, M. F. Adasme, M. Schroeder, *Nucleic Acids Res* **2015**, *43*, W443-447.
- [21] a) P. A. Kollman, I. Massova, C. Reyes, B. Kuhn, S. Huo, L. Chong, M. Lee, T. Lee, Y. Duan, W. Wang, O. Donini, P. Cieplak, J. Srinivasan, D. A. Case, T. E. Cheatham, 3rd, *Acc Chem Res* **2000**, *33*, 889-897; b) R. Kumari, R. Kumar, C. Open Source Drug Discovery, A. Lynn, *J Chem Inf Model* **2014**, *54*, 1951-1962.
- [22] a) M. Karplus, J. N. Kushick, *Macromolecules* **1981**, *14*, 325-332; b) S. Kassem, M. Ahmed, S. El-Sheikh, K. H. Barakat, *J Mol Graph Model* **2015**, *62*, 105-117; c) J. Zhang, H. Zhang, T. Wu, Q. Wang, D. van der Spoel, *J Chem Theory Comput* **2017**, *13*, 1034-1043.
- [23] A. Koeberle, U. Siemoneit, U. Buhring, H. Northoff, S. Laufer, W. Albrecht, O. Werz, *J Pharmacol Exp Ther* **2008**, *326*, 975-982.
- [24] A. Koeberle, U. Siemoneit, H. Northoff, B. Hofmann, G. Schneider, O. Werz, *Eur J Pharmacol* **2009**, *608*, 84-90.
- [25] F. Rorsch, I. Wobst, H. Zettl, M. Schubert-Zsilavecz, S. Grosch, G. Geisslinger, G. Schneider, E. Proschak, *J Med Chem* **2010**, *53*, 911-915.
- [26] B. Waltenberger, K. Wiechmann, J. Bauer, P. Markt, S. M. Noha, G. Wolber, J. M. Rollinger, O. Werz, D. Schuster, H. Stuppner, *J Med Chem* **2011**, *54*, 3163-3174.
- [27] S. He, C. Li, Y. Liu, L. Lai, *J Med Chem* **2013**, *56*, 3296-3309.
- [28] R. A. Friesner, J. L. Banks, R. B. Murphy, T. A. Halgren, J. J. Klicic, D. T. Mainz, M. P. Repasky, E. H. Knoll, M. Shelley, J. K. Perry, D. E. Shaw, P. Francis, P. S. Shenkin, *J Med Chem* **2004**, *47*, 1739-1749.
- [29] T. A. Halgren, R. B. Murphy, R. A. Friesner, H. S. Beard, L. L. Frye, W. T. Pollard, J. L. Banks, *J Med Chem* **2004**, *47*, 1750-1759.
- [30] A. Gaulton, L. J. Bellis, A. P. Bento, J. Chambers, M. Davies, A. Hersey, Y. Light, S. McGlinchey, D. Michalovich, B. Al-Lazikani, J. P. Overington, *Nucleic Acids Res* **2012**, *40*, D1100-1107.
- [31] Schrödinger Release 2016-2: Canvas, LLC, New York, NY, 2017.
- [32] Schrödinger Release 2016-2: LigPrep, LLC, New York, NY, 2017.
- [33] J. C. Shelley, A. Chollet, L. L. Frye, J. R. Greenwood, M. R. Timlin, M. Uchimaya, *J Comput Aided Mol Des* **2007**, *21*, 681-691.
- [34] Schrödinger Release 2016-2: Glide, LLC, New York, NY, 2017.
- [35] Schrödinger Release 2016-3: Desmond Molecular Dynamics System, New York, NY, 2016. Maestro-Desmond Interoperability Tools, Schrödinger, New York, NY, 2016.
- [36] Schrödinger Small-Molecule Drug Discovery Suite 2016, LLC, New York, NY, 2017.
- [37] M. A. Lomize, A. L. Lomize, I. D. Pogozheva, H. I. Mosberg, *Bioinformatics* **2006**, *22*, 623-625.
- [38] M. J. Abraham, T. Murtola, R. Schulz, S. Pall, J. C. Smith, B. Hess, E. Lindahl, *SoftwareX* **2015**, *1-2*, 19-25.
- [39] C. J. Dickson, B. D. Madej, A. A. Skjerve, R. M. Betz, K. Teigen, I. R. Gould, R. C. Walker, *J Chem Theory Comput* **2014**, *10*, 865-879.
- [40] J. Wang, W. Wang, P. A. Kollman, D. A. Case, *J Mol Graph Model* **2006**, *25*, 247-260.
- [41] A. W. Sousa da Silva, W. F. Vranken, *BMC Res Notes* **2012**, *5*, 367.
- [42] N. A. Baker, D. Sept, S. Joseph, M. J. Holst, J. A. McCammon, *Proc Natl Acad Sci U S A* **2001**, *98*, 10037-10041.
- [43] a) M. Jafari, F. Mehrnejad, R. Aghdami, N. Chaparzadeh, Z. Razaghi Moghadam Kashani, F. Doustdar, *J Chem Inf Model* **2017**, *57*, 929-941; b) J. Lee, S. W. Jung, A. E. Cho, *Langmuir* **2016**, *32*, 1782-1790.

Entry for the Table of Contents



Novel scaffolds offer new hope against inflammation: Many pathological conditions involve inflammation, including rheumatoid arthritis, asthma and cancer. mPGES-1, a safer alternative to COX inhibition, represents an attractive therapeutic target for inflammation-related diseases. By using VS approaches and small library synthesis, we hereby identified novel scaffolds that warrant further chemical development as non-acidic mPGES-1 inhibitors.